MEMS Fault Model Generation using CARAMEL[1]

Abhijeet Kolpekwar, Chris Kellen, and R. D.(Shawn) Blanton

ECE Department
Carnegie Mellon University
Pittsburgh, PA 15213-3890

ABSTRACT

*We have enhanced the process simulator CODEF [2] into a tool called CARAMEL (**C**ontamination **A**nd **R**eliability **A**nalysis of **M**icro**E**lectromechanical **L**ayout) for analyzing the impact of contamination particles on the geometrical and material properties of microelectromechanical systems (MEMS). CARAMEL accepts as input a microelectromechanical layout, a particulate description, and a process recipe. CARAMEL produces a mesh description of the defective layout that is completely compatible with the electromechanical simulator ABAQUS [31]. Analysis of CARAMEL's output indicates that a wide range of defective structures are possible due to the presence of contaminations. Moreover, electromechanical simulations of CARAMEL's mesh representations of defective layout has revealed that a wide variety of faulty behaviors are associated with these defects. In this paper, we describe CARAMEL and its application to the development of realistic fault models for MEMS.*

1 Introduction

MEMS are miniature electromechanical sensor and actuator systems developed from the mature batch-fabricated processes of VLSI technologies. The dramatic improvement in the performance-to-cost ratio, reliability, and functionality over conventional counterparts has escalated the demands for MEMS-based products. There are many emerging research areas that exploit the spectrum of functionality made possible by MEMS. The most advanced and successful MEMS area of application include sensors and actuators systems for automotive airbag accelerometers. But many more applications are expected in many diverse areas such as process control and biomedical engineering.

[1]This research effort is sponsored by the National Science Foundation under grant MIP-9702678 and the Defense Research Projects Agency under Rome Laboratory, Air Force Materiel Command, USAF, under grant F30602-97-2-0323.

There are three categories of fabrication processes for MEMS: Surface micromachining, bulk micromachining and high level aspect-ratio lithography [1]. Advances in all these categories have made it possible to develop high quality MEMS. Technology advances however have not positively impacted the design cycle for MEMS, which is still currently measured in years. In order to keep pace with technology advances, CAD tools tailored for MEMS design and verification are essential.

The development and deployment of new MEMS products will not occur due to advances in design, packaging, and processing alone. Testing methodologies must be developed in concert that are capable of assessing faulty behavior (in the form of fault simulation and automatic test pattern generation) along with design for testability (DFT) structures that improve and ensure the end quality of MEMS-based products. It should also be noted that many new and existing MEMS applications are integral parts of safety-critical systems. Consequently, the need to address reliability of MEMS makes the testability problem that much more important. To ensure high quality and reliability of MEMS based devices, a comprehensive testing methodology must be developed that allows devices to be tested economically with a very high level of confidence. Success of any testing methodology is highly dependent on the fault models employed. Fault models that do not "cover" real defective behavior can reduce defect coverage and degrade test quality. The work presented in this paper addresses this need.

MEMS fault models, unlike their digital and analog counterparts, must explicitly consider the impact of defects on the micromechanical structures. Our approach towards developing effective MEMS fault models centers on the inductive generation of the possible faulty behaviors from realistic contamination simulations. We have chosen the folded-flexure comb-drive microresonator[2] as our research vehicle because it possesses many of the basic structures (beams, joints,

springs, etc.) that many researchers believe will form the core primitives of a MEMS design library [3, 4, 5]. The hope is that the resulting information will provide the basis for developing a generic fault model that is applicable to the class of surface-micromachined MEMS.

Our experience is that a major cause of faulty behavior in MEMS is due to particulate contaminations that occur during various process steps of fabrication [7]. Contaminations can cause a significant perturbation in the structural and material properties of the microstructure [6]. Thus, a formal assessment of both the possible defective structures and the corresponding faulty behaviors on MEMS design primitives will lead to the formation of effective MEMS fault models. Such fault models will undoubtedly lead to methods for fault grading, test generation, DFT and design for fault avoidance. The fault modeling process can also be used to form links between defects and faulty behaviors. Such links would aid in diagnosis by helping identify the process steps that are likely to produce the observed faulty behavior [8].

We have enhanced the process simulator CODEF [2] into a tool called CARAMEL (Contamination And Reliability Analysis of MicroElectromechanical Layout) for analyzing the impact of contamination particulates on the properties of microelectromechanical layout. CARAMEL is an integral component of our MEMS fault model generation (see Figure 1). CARAMEL requires three inputs:

1. **Design definition:** This is typically a layout of the design in the Caltech Intermediate Form (CIF).

2. **Process definition:** This includes a sequence of process steps with all the required details such as deposition thickness, etching rate, etching time, etc.

3. **Contamination definition:** This includes geometrical and material characteristics of the particulate contamination, its location in the MEMS layout, and its process step of introduction.

CARAMEL performs process simulation and creates a three-dimensional representation of the defective microelectromechanical layout. It then extracts a mesh representation from the defective layout whose form is completely compatible with the mechanical simulator ABAQUS [31]. Mechanical simulation of the mesh then allows us to link the contamination of concern to a defective structure and a faulty behavior. Observed faulty behaviors are then classified and used to form models at the next level of abstraction. Monte Carlo iteration around the flow of Figure 1 provides a mechanism for creating realistic fault models for MEMS.

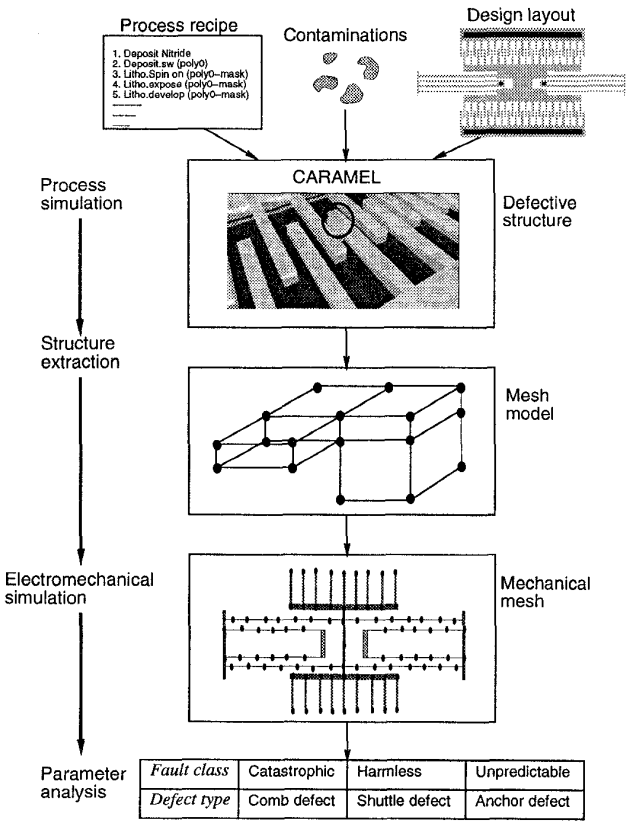

Figure 1: MEMS contamination analysis using CARAMEL.

In this paper, we describe CARAMEL and illustrate its use in MEMS fault model generation. The resonator structure under consideration belongs to a class of MEMS known as surface-micromachined MEMS. Prototype surface micromachining processes are available from MCNC (Multi-user MEMS Processes service (MUMPs) [9]), Analog Devices' iMEMS process, and from Sandia National Labs. We have selected the MUMPs process for the contaminations simulations of the resonator due to its open availability. In this process, thin films are sequentially deposited and patterned on top of the substrate. The

[2]In the remaining parts of this paper, we will refer to the folded-flexure comb-drive microresonator simply as the "resonator".

movable MEMS structure is created when a "release" step is used to etch away a sacrificial layer. The seminal paper on the resonator is given in [10]. Analytic models of the resonator's pertinent characteristics can be found in [11, 12, 13]. The resonator structure is a mature case study in the design of "suspended MEMS" which are now used in commercial accelerometers [15, 16], gyroscopes (soon), and micromirror optical beam steering [17]. Future commercial applications are in resonator-based oscillators [18], IF mixers, high-Q IF filters for communications, and microstages for probe-based data storage [19].

The rest of this paper is organized as follows. Section 2 describes prior work in the area of MEMS testing. Section 3 describes MEMS contamination analysis using our tool CARAMEL. In Section 4, simulation results obtained using CARAMEL on the surface-micromachined microresonator are presented. Finally in Section 5, we present conclusions and outline areas of future work.

2 Related Work

Most work in the MEMS area centers on design, technology, and packaging problems and not testing. However, there are a number of researchers that are concerned with MEMS testability [20, 21, 22]. In this section, we discuss the previous work performed in this area.

In [20], Olbrich and others have outlined challenges associated with MEMS testing and demonstrated their testing approach on a bulk-micromachined accelerometer. They use an electrical schematic to model both the electrical and mechanical components of the accelerometer. Similar to digital ICs, they model defects using stuck-at, bridging, and stuck-open faults. Carefully placed resistors are added to their electrical schematic to model these faults. An additional level of complexity is considered by allowing the parameter values of these "fault" resistors to vary. They use exhaustive Hspice simulations to determine which voltage and current nodes are good candidates for observing faulty behavior.

Vermeiren and his colleagues in [21] stress the importance of the MEMS model and its relationship to defects. They also use an electrical model to represent both the mechanical and electrical components of MEMS. However, the model is constructed in a such way so as to allow the accurate modeling of a wide variety of MEMS defects.

Similar to [20], Lubaszewski et. al. [22] provide an extensive overview of the issues and possible solutions for the problems related to MEMS fault modeling, simulation, test generation, DFT, and BIST. They also described their MEMS testing environment termed CAT (Computer-Aided Testing). Similar to [20] and [21], they use an electrical schematic to model MEMS structures. MEMS defects are modeled using the concept of *mutants* and *saboteurs*. Mutants are used to represent MEMS defects that cause parametric changes in existing model components. Saboteurs, on the other hand, cause components to be removed and added to the electrical model to represent defects that add or remove elements from the MEMS microstructure. The mutant/saboteur concepts are used in the CAT environment to illustrate fault simulation and test pattern generation for a MEMS electro-thermal converter.

Unfortunately, none of these works have discussed or presented a general methodology for coping with the mechanical defects directly. This is important since a loss of modeling accuracy may be incurred if mechanical defects are forced into an electrical model. Modeling the mechanical defects accurately requires an understanding of their impact on the behavior of MEMS devices. This understanding requires one to analyze a wide range of defective microelectromechanical structures. Lack of such information can result in poor-quality fault models. Our work mainly focuses on exploring MEMS behavior under mechanical defects. Using CARAMEL, we generate a broad spectrum of faulty microstructures and analyze their effects on the functionality of the MEMS device through low-level mechanical simulations. It is believed that the results of these simulations will allow a systematic fault categorization, thus forming the basis of MEMS fault models which will ultimately lead to an effective test methodology for MEMS.

3 CARAMEL

CARAMEL is a process simulator that maps particle contaminations to defective microstructures. It is built around the tool CODEF, which is a contamination-to-defect-to-fault mapper for pure electrical layouts [2]. Described next are the three phases of CARAMEL's operation.

3.1 Process Simulation

This phase of CARAMEL maps spot contaminations to layout defects and is implemented using a modified version of CODEF. CODEF determines the impact of a particle on the contaminated region of the IC layout. It accepts layout information, a process description, and contamination statistics for each processing step of interest. CODEF allows for the exact characteristics of the contamination particle to be simulated including the particle's size, density, conduc-

tivity, and fabrication step of introduction. Given the contamination parameters, it simulates all the fabrication steps and creates a three-dimensional (3D) structure of the defective device. CODEF, in its unmodified form, is used to analyze the effects of particles on an electrical IC layout. It utilizes a circuit extractor which traverses the 3D structure to create a SPICE netlist. Defective circuit behavior resulting from the contaminations can then be analyzed through SPICE simulations.

To make use of CODEF for MEMS contamination analysis, we have defined a complete MUMPs fabrication process as a sequence of steps in the PREDITOR format [26]. The MUMPs process is used to form micromechanical structures composed of thin films formed on the surface of the substrate. These thin-film microstructures are called surface micromachined MEMS. Because the resonator is a single-polysilicon structure, fabrication of the resonator utilizes only a subset of the complete three-polysilicon MUMPs process. This simplified version of the MUMPs process is described in [27] and is illustrated in Figure 2. First, a low-stress silicon nitride is deposited on the silicon substrate to provide electrical isolation between microstructures. An electrical interconnection layer of polysilicon is then deposited and patterned. Next, a 2 μm-thick layer of phosphosilicate glass (PSG) is deposited. PSG acts as sacrificial spacer layer for the microstructures. After contact cuts are made in PSG, a 2 μm-thick layer of polysilicon is deposited and patterned to form a microstructure. A final wet etch in hydrofluoric acid (HF) dissolves the PSG and releases the microstructure so that it is free to move. Contact cuts in the PSG are anchor points that fix the microstructure to the substrate.

In CARAMEL, we have modified CODEF to handle the MUMPs "release" step (i.e. the HF etch of PSG) as described above. Adding this step, which is not part of any standard CMOS process, allows us to perform MUMPs process simulations using realistic contaminations.

3.2 Structure Extraction

The structure extraction phase produces a 3D mesh representation of the defective structure generated by CODEF. Mechanical simulation of the mesh (using finite element analysis (FEA) tools like ABAQUS [31]) allows detailed analysis of the effects of contaminations on the mechanical structure.

The process simulator creates a 3D representation of the resonator structure consisting of hierarchically connected layers of material known as the Chip Data Base (CDB) [28]. CDB is created from the MUMPS process flow and the CIF layout of the resonator. In addition, contamination particles may be introduced at random locations in the process flow, under control of the process simulator, which can alter the final 3D structure of the resonator structure. CARAMEL creates a separate "mesh database" from the CDB to represent the MEMS structure as a set of two-dimensional (2D) corner-stitched rectangular regions [29]. Each region of the mesh consists of a set of material elements. However, the mesh database differs from a traditional corner-stitched database because elements in the former are allowed to be less than maximal width. This is a necessary feature since the mesh used for mechanical simulation requires that each region have a single neighbor or no neighbor along each of its edges. Each element also has associated data that describes its material characteristics, its position in the z direction, and a flag that indicates if the base of the element is anchored.

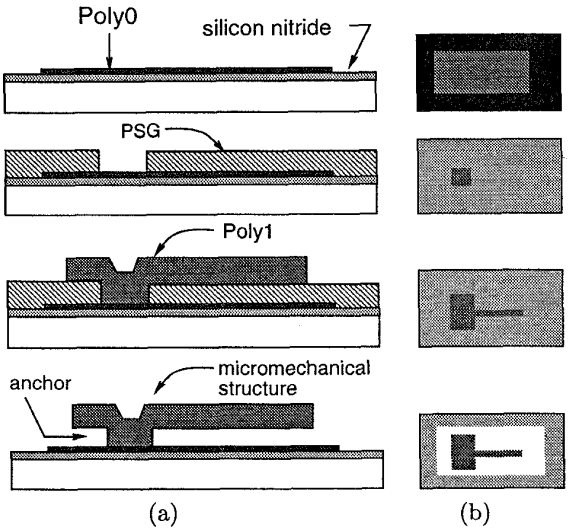

Figure 2: Abbreviated flow for MCNC's MultiUser MEMS Process service [27]: (a) Cross-sectional view. (b) Top view (layout).

The MEMS meshing phase:

1. Creates a corner-stitched database containing the regions to be simulated.
2. Determines the connectivity of the regions.
3. "Splits" the mesh database to ensure that each region has only one or zero neighbors in the x, y and z directions.

4. Identifies the elements and generates node numbers for all the vertices of every region. (This is required by the FEA tool for mechanical simulation.)

5. Generates the final mesh input model for the FEA tool.

Mesh Database Creation

The mesh database for the resonator consists only of polysilicon one (POLY1) and defect material, i.e., the material of the particle contamination. The mesh is created by examining every region of CODEF's CDB. Each element of POLY1 or defect material is added to the mesh database along with a flag indicating if the element is fixed to some other material or contains free space underneath. The flag information is used later to determine which elements are free to move.

Determining Element Connectivity

Understanding the behavior of the resonator requires mechanical simulation of its moving parts. The moving parts of the resonator includes the mass shuttle and everything connected to the shuttle. Because a particle contamination can alter the topography of the resonator, the resulting defective structure must be derived from the CDB of elements. In this phase, CARAMEL determines all the connected elements from a a user-specified element on the resonator's layout. A simple algorithm is employed that marks the user-specified element and continues to mark neighboring elements until all connected regions are marked.

Element Splitting

The mechanical mesh required by FEA tools must be constructed so that adjacent regions meet only at region vertices (nodes). CARAMEL must meet this adjacency constraint not only in the x and y directions but also in the z-direction.

- **x-y splitting:** In a standard corner-stitched database, a region edge can have multiple neighboring regions or a partial neighbor as shown in Figure 3a. Such a situation violates the constraint described above for the mechanical mesh. The x-y splitting operation modifies an element so that every region edge has a single neighboring element or no neighbor at all. Splitting is performed by analyzing the edge neighbors of every region in the CDB. For each edge that violates the constraint, the current region is split at the neighbor's edge. (See Figure 3.)

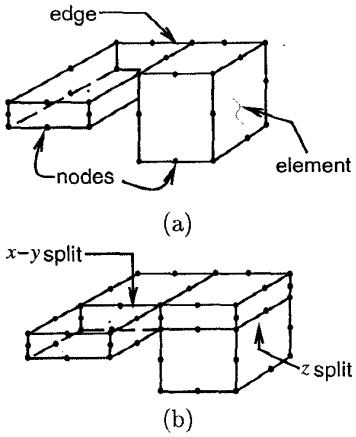

Figure 3: Illustration of element splitting for mechanical mesh construction: (a) A set of regions before split and (b) the same regions after x-y and z splits.

- **z splitting:** In an analogous way, elements may need to be split in the z direction as well. In this case, adjacent regions that have elements of differing heights must be split in the z direction so that the resulting elements share nodes. This is accomplished using a simple algorithm that compares the top and bottom coordinates of an element with all its neighboring elements. If an adjacent element is contained in the current element, the current element is split. (See Figure 3.) There is one exception to the z-split operation when the element of concern is fixed. Typically, split elements inherit identical properties (material, conductivity, etc.) from the original element. In the case of fixed elements, only the newly-created bottom-half element is fixed.

The result of CARAMEL's extraction phase is a mechanical mesh that is directly compatible with the FEA tool ABAQUS. The resulting mechanical mesh captures the impact of the particle contamination on both the electrical and mechanical properties of the resonator. It should be noted here that CARAMEL is a general tool and is therefore not restricted to the resonator but is applicable to any generic MEMS layout. It is therefore possible to analyze the impact of particle contaminations on a wide variety of MEMS topologies. In the next section, we examine the impact of 721 contaminations on the structure and behavior of the resonator.

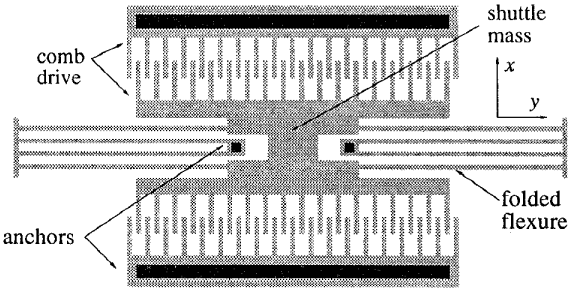

Figure 4: Top view of a comb-drive microresonator.

4 Simulation Results

CARAMEL was used to analyze 721 unique contaminations of the resonator. We analyzed contaminations of various sizes and material properties. In addition, contaminations were placed at many different resonator locations and were introduced at many different steps of the MUMPs process. Out of 721 contaminations, 263 were physically in contact with the resonator structure. The effect of each of these 263 contaminations was observed at each phase of CARAMEL's operation. The mechanical simulator ABAQUS was also used to compute the resonant frequency of each of the mechanical meshes generated by CARAMEL. The resonant frequency is analyzed because it is one of the crucial parameters for determining if the resonator is functioning properly [7]. In Table 1, we provide details of five representative cases of the contamination analysis. Note that the first entry of Table 1 gives the resonant frequency for the defect-free resonator. For each of the five defects considered, we provide the location of the contamination (Table 1), the resulting 3D defective structure (Figure 5), top view of the mechanical mesh (Figure 5) and the resulting resonant frequency reported by ABAQUS (Table 1).

- **Comb Defect:** Figure 5a shows the impact of a contamination located between adjacent comb fingers. The process simulation phase of CARAMEL reveals that the contamination welds together the two normally-moving fingers. The fixed fingers transforms the two comb drives into a single structure thereby changing the mesh model required for mechanical simulation. Mechanical simulation of a defect-free resonator requires only the shuttle and flexure. The result obtained from mechanical simulation shows a 29% increase in resonant frequency; an indication that this defect has caused a catastrophic failure.

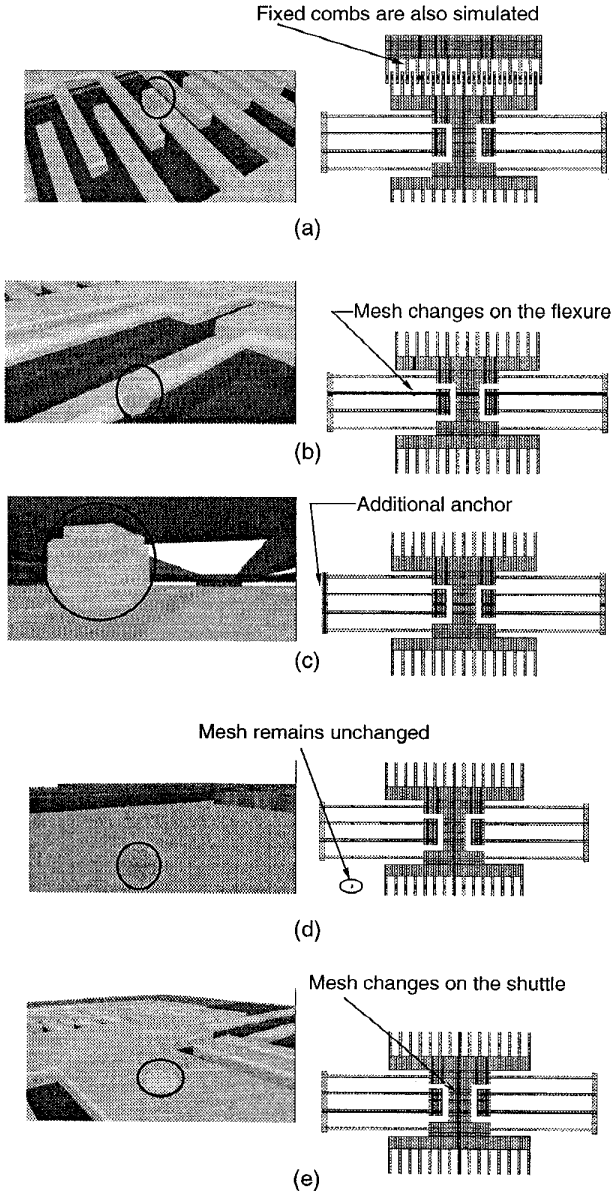

Figure 5: Three-dimensional representations of defective resonators and their corresponding mechanical mesh for a particle contamination located (a) between adjacent comb fingers, (b) on a beam, (c) under the shuttle, (d) outside of the resonator's active area and (e) on the shuttle.

Particle location	Diameter size (μm)	Density (kg/m^3)	Added after step #	Resonant frequency (Hz)	Percentage change in f_x (%)
None	-	-	-	69772	
Comb	2.4	2330	Poly1 deposition	90116	+29.2%
Beam	1.5	2330	PSG deposition	68646	-1.61%
Shuttle-1	2.0	2330	Poly0 PR Strip	88328	+26.6%
Outside	2.0	2330	Poly0 deposition	69772	0%
Shuttle-2	1.5	2330	PSG deposition	69721	≈0%

Table 1: Five representative cases of defect analysis using CARAMEL.

- **Beam Defect:** The impact of a defect affecting a beam of the folded-flexure is illustrated in Figure 5b. Such a contamination results in a slightly heavier beam. The increased mass of the beam changes the resonant frequency by -1.61% . Note the meshing complexity of the area surrounding the defect's location. The increased "meshing" is a reflection of the number of splits required to accurately represent the region containing the defect.

- **Shuttle-1 Defect:** A contamination that becomes lodged between the resonator and the substrate acts as an anchor. CARAMEL handles such cases by defining an anchor element at the contamination location during the extraction phase. The meshing phase discovers that the contaminant is connected to the suspended structure and the substrate surface. The resulting mesh used in the mechanical simulation therefore has an extra anchor. The impact of such a defect is shown in Figure 5c. Simulation of the corresponding mesh indicates that the resonant frequency has increased significantly, which is quite intuitive since the resonator is now fixed to the substrate at an additional location.

- **Outside Defect:** Contaminations lying outside the structure are treated like the others, but during the "connectivity" phase of meshing, it is determined that the contaminant is not connected to the structure of interest. Meshes for such defects are generated but are not simulated. For these cases the nominal values of resonant frequency are reported. An example of this type of harmless defect is illustrated in Figure 5d.

- **Shuttle-2 Defect:** Figure 5e shows another interesting case where the contamination becomes totally encapsulated by the shuttle mass. Process simulation indicates that a small bump is formed on the shuttle surface. The creation of such a bump changes the meshing of the affected region evidenced by the dense meshing surrounding the defect area. Mechanical simulation reveals a very small decrease in resonant frequency due to the additional mass.

The five analyzed cases demonstrate CARAMEL's ability to model and simulate a variety of contamination effects on the MEMS microstructure. The tool can be effectively used to generate several thousand contamination simulations under a Monte-Carlo mode of operation. In Monte Carlo mode, contaminations are introduced into the process at random steps, with random sizes, and at random locations in the layout. Such analysis can produce the full spectrum of MEMS failure modes. The observed deviations in behavior can then be systematically categorized under various fault classes. These fault classes can then be mapped to appropriate fault models at the higher level of abstraction. In other words, such an analysis provides a technique for abstracting defective beams, gaps, shuttles, etc. into higher-level fault models. We have performed 721 simulations using CARAMEL to illustrate its Monte-Carlo mode of operation. Process simulation showed that only 263 contaminants were in physical contact with the microstructure. Mechanical simulation showed that 65 of the 263 simulations produced defective structures that significantly altered the resonant frequency of the resonator.

Table 2 presents a coarse fault categorization of the 263 defects. The three broad fault classes are identified as catastrophic, parametric, and harmless. *Catastrophic* defects are those defects that cause more than a 30% change in the resonant frequency f_x. Defects that cause a frequency deviation between 5% and 30% are termed *parametric*. Defects are termed *harmless* if they have a negligible affect on f_x.

More details about the defects are provided in Table 3. It shows the occurrences of defects with respect to its process step of introduction. This information indicates which MUMPs process steps are most vul-

Defect type	Number of occurrences	Deviations in f_x	Comments
Catastrophic	47	$\Delta f_x > 30\%$	Resonator functionality is completely destroyed.
Parametric	18	$5\% \leq \Delta f_x \leq 30\%$	Resonator still works but with large deviations from the desired functionality.
Harmless	198	$\Delta f_x < 5\%$	Resonator functionality within specifications.

Table 2: Coarse fault categorization based on deviation in resonant frequency f_x.

Particle location	Catastrophic faults (%)	Parametric faults (%)	Total (%)
Shuttle	31.9	33.3	32.3
Comb fingers	42.6	16.7	35.4
Folded flexure	25.5	50.0	32.3

Table 4: Spatial distribution of faults in the microresonator.

nerable to particle contaminations. It can be seen that step 8 (i.e. Etch Poly0 resist) is highly prone to catastrophic failures. This result is quite intuitive. Poly0 forms the base of the resonator while the "suspended' structure is built from Poly1. Hence, any contamination occurring on Poly0 can bind the two layers and impede resonator movement. This situation often leads to catastrophic failures. Thus, the Poly0 deposition and development phases of fabrication are quite vulnerable to particle contaminations. As indicated in Table 3, contaminations introduced during this phase (steps 3 to 12) lead to over 60% of the catastrophic failures observed.

Table 4 shows the spatial distribution of the contaminations over the resonator layout that caused catastrophic and parametric failures. It can be observed that the comb fingers are the most defect-prone region in the resonator causing around 43% of the total number of catastrophic faults. Defects affecting the combs have resulted in significant changes in the resonant frequency. The shuttle, due to its relatively large area, is quite susceptible to being "hit" by a contamination; however for the same reason the changes in the shuttle do not affect the resonator operation. The smaller surface area of the folded-flexure beams, on the other hand, is less likely to be affected. However, when the beams are impacted, their behavior is significantly disturbed.

It is also important to note that all the catastrophic failures due to shuttle contaminations occur before deposition of the Poly1 layer. These contaminations are lodged between the Poly1 and Poly0 layers creating an anchor effect. Conversely, contaminations occurring on the shuttle after/during Poly1 deposition do not cause appreciable change in the resonant frequency. Thus, contamination impact on resonator behavior is a function of *both* the location and process step in which it is introduced.

Following are the main observations that can be drawn from the simulation results:

1. Particle contaminations have a large impact on the resonator functionality and the resulting spectrum of faulty behaviors can be discovered through contamination and FEM simulations.

2. A systematic classification of the faulty behavior can be made by mapping various fault classifications to a higher level of abstraction.

3. Impact of particle contamination is a function of both the location and process step in which it is introduced.

4. The comb drive is the most defect prone region of the resonator and the Poly0 deposition process is the most vulnerable to a contamination.

5 Conclusions and Future Work

We have automated the contamination analysis process for microelectromechanical layout using our tool CARAMEL. CARAMEL can be effectively used to directly investigate the faulty behavior of defective MEMS structures. Here, we have illustrated CARAMEL's use on a folded-flexure resonator. Analysis of 721 different defects indicates that spot contaminations can have a significant impact on the behavior of the resonator. Moreover, the results show that the impact of a particular defect is highly dependent upon *where* it is located in the resonator's layout

Process step	Number of occurrences	% of occurrences causing faults	Catastrophic faults	Parametric faults
1 (Initialize)	13	30.8	2	2
2 (Nitride deposit)	9	44.4	3	1
3 (Poly0 deposit)	16	68.8	9	2
4 (Litho spinon Poly0)	3	33.3	1	
5 (Litho expose Poly0)	3	66.7		2
6 (Litho develop Poly0)	4	100	4	
7 (Etch Poly0)	4	25.0	1	
8 (Etch Poly0 resist)	14	85.7	12	
9 (PSG deposit)	2	100	2	
12 (Litho develop PSG)	2	0.0		
13 (Etch PSG)	1	0.0		
19 (Etch Anchor1 resist)	3	0.0		
20 (Poly1 deposit)	31	12.9	4	
21 (Litho spinon Poly1)	29	13.8	4	
22 (Litho expose Poly1)	26	11.6	3	
23 (Litho develop Poly1)	22	4.6	1	3
24 (Etch Poly1)	19	10.5		2
25 (Etch Poly1 resist)	38	15.8	1	5
48 (PSG release)	24	4.2		1
Total defects	263		47	18

Table 3: Defect categorization based on the MUMPs process step for which the contamination was introduced.

and *when* it is introduced into the manufacturing process. Currently we are addressing the following issues to improve CARAMEL for MEMS fault model generation:

- **Mesh Optimization:** Presently, the mechanical mesh generated by CARAMEL is not optimized in anyway. It contains many artifacts from the original process simulation that add to the size and complexity of the mesh. We plan to optimize the mesh in order to accelerate the mechanical simulation phase.

- **Automatic Fault Categorization:** We plan to have CARAMEL sort through the large amount of simulated data and extract the unique faults. This will reduce the amount of mechanical simulation required for fault categorization.

- **Simulation Complexity:** We are currently simulating static structures that do not change during the course of simulation. Static structures do not capture a number of interesting and possibly important defects. For example, a particle located between but not touching the comb finger may limit the motion of the resonator. This and other types of interactions will require more knowledge of the material properties of the contaminants but can be modeled using our approach.

References

[1] C. H. Mastrangelo and W.C. Tang, "Sensor Technology", Chapter 2, *Semiconductor Sensors*, S.M. Sze, Ed., New York, John Wiley & Sons, Inc., 1994.

[2] J. Khare and W. Maly, "From Contamination to Defects, Faults and Yield Loss", *Kluwer Academic Publishers*, Boston, 1996.

[3] R. D. Blanton, G. K. Fedder and T. Mukherjee, "Hierarchical Design and Test of MEMS", *Microsystem Technology News*, pp. 28-31 April 1998.

[4] G. K. Fedder, S. Iyer and T. Mukherjee, "Automated Optimal Synthesis of Microresonators", *Technical Digest of IEEE International Conference on Solid State Sensors and Actuators*, Vol. 2, pp. 1109-1112, June 1997.

[5] T. Mukherjee and G. K. Fedder, "Structured Design of Microelectromechanical Systems", In *Proc. 34th Design Automation Conference*, pp. 687-685, June 1997.

[6] A. Kolpekwar, R. D. Blanton "Development of MEMS Testing Methodology" In *Proc. of International Test Conference*, pp. 923-931, Nov. 1997.

[7] A. Kolpekwar, R. D. Blanton and D. Woodilla "Failure Modes for Stiction in Surface-Micromachined MEMS" In *Proc. 1998 International Test Conference*, Oct. 1998.

[8] J. Khare and W. Maly and N. Tiday, "Fault Characterization of Standard Cell Libraries Using Inductive

Contamination Analysis (ICA)" In *Proc. 14th VLSI Test Symposium*, pp. 405-413, April 1997.

[9] D. A. Koester, R. Mahadevan and K. W. Markus, "Multi-
user MEMS Processes (MUMPS): Introduction and Design Rules", http://mems.mcnc.org/mumps.html, Oct. 1994.

[10] W. C. Tang, T. C. H. Nguyen, M. W. Judy and R. T. Howe, "Electrostatic Comb Drive of Lateral Polysilicon Resonators", *Sensors and Actuators A*, Vol. 21, Nos. 1-3, pp. 328-331, Feb. 1990.

[11] G. K. Fedder, *Simulation of Microelectromechanical Systems* PhD thesis, University of California at Berkeley, Sept. 1994.

[12] Z. Zhang and W. C. Tang, "Viscous Air Damping in Laterally Driven Microresonators", In *Proc. IEEE Micro Electro Mechanical Systems Workshop*, pp. 199-204, Jan. 1994.

[13] W. A. Johnson and L. K. Warne, "Electrophysics of Micromechanical Comb Acutators", *Journal of Microelectromechanical Systems*, Vol. 4, No. 1, pp. 49-59, March 1995.

[14] R. E. Harr, "Design for Large Scale Integration of Mixed Technology Microdevices", *R & D Program of DARPA, ETO*, 3701 North Fairfax Drive, Arlington VA 22203-1714, 1996.

[15] Analog Devices Inc., "ADXL Series Accelerometer Datasheets", One Technology Way, P.O. Box 9106, Norwood, MA 02062-9106, 1996.

[16] Motorola, "MMAS40G10D Accelerometer Datasheet", Semiconductor Products Sector, 6501, William Cannon Drive, Austin TX, 1996.

[17] M. A. Mignardi, "Digital Micromirror Array for Projection TV", *Solid State Technology*, Vol. 37, No. 7, pp. 63-64, July 1994.

[18] C. T. C. Nguyen and R. T. Howe, "CMOS Micromechanical Resonator Oscillator", In *Technical Digest of the IEEE Int. Electron Devices Meeting*, pp. 199-202, 1993.

[19] G. K. Fedder, S. Santhanam, M. L. Reed, S. Eagle, D. Guillou, M. S.-C. Lu and L. R. Carley, "Laminated High-Aspect-Ratio Microstructures in a Conventional CMOS Process", In *Proc. IEEE Micro Electro Mechanical Systems Workshop*, pp. 13-18, Feb. 1996.

[20] T. Olbrich, A. Richardson, W. Vermeiren, B. Straube, "Integrating Testability into Microsystems", *Microsystem Technologies*, pp. 72-79, Feb. 1997.

[21] W. Vermeiren, B. Straube, A. Holubek, "Defect-Oriented Experiments in Fault Modeling and Fault Simulation of Microsystem Components", In *Proc. European Design and Test Conference,* March 1996.

[22] M. Lubaszewski, E. F. Cola and B. Courtois, "Microsystem Testing: An Approach and Open Problems" In *Proc. Design and Test in Europe,* Feb. 1998.

[23] H. V. Allen, S. C. Terry, D. W. DeBruin, "Accelerometer Systems with Self-testable Features", *IEEE Transactions on Sensors and Actuators*, pp. 153-161, 1989.

[24] J. Bryzek, "New Technologies for Silicon Accelerometers Enable Automotive Applications", Lucas Nova Sensors, SAE 920474, pp. 25-32.

[25] L. Zimmermann, "A Microsystem including a Silicon Capacitive Accelerometer, CMOS Switched-Capacitor Electronics and True Self-Test Capability", *IEEE Transactions on Sensors and Actuators*, pp. 190-195.

[26] D. M. H. Walker, C. S. Kellen and A. J. Strojwas, "The PREDITOR Process Editor and Statistical Simulator" In *Proc. 1991 International Workshop on VLSI Process and Device Modeling*, pp. 120-123, May 1991.

[27] G. K. Fedder and T. Mukherjee, "Physical Design for Surface-Micromachined MEMS", In *Proc. 5th ACM/SIGDA Physical Design Workshop*, pp. 53-60, April 1996.

[28] D. M. H. Walker, C. S. Kellen, D. M. Svoboda, and A. J. Strojwas, "The CDB/HCDB Semiconductor Wafer Representation Server", *IEEE Transactions on Computer-Aided Design of Integrated Circuits and Systems,* Vol. 12, No. 2, pp. 283-95, Feb. 1993.

[29] J. K. Ousterhout, "Corner Stitching: A Data-Structuring Technique for VLSI ", *IEEE Transactions on Computer-Aided Design of Integrated Circuits and Systems*, Vol. 3, No. 1, pp. 87-100, Jan. 1984.

[30] Sandia National Laboratories, "Intelligent MicroMachine Initiative" P.O. Box 969, Livemore, CA 94551.

[31] Hibbit, Karlsson & Sorensen, Inc., "ABAQUS User Manual", Vol. 2, Pawtucket, RI, 1995.